# Validation of XFEM-based Simulation Capabilities for Fluid-driven Fractures in Permeable Media

Sandeep Kumar, Kevin H. Searles and Shekhar V. Gosavi

ExxonMobil Upstream Research Company

22777 Springwoods Village Pkwy, Spring, Texas, USA

***ABSTRACT:*** *The eXtended Finite Elements Method (XFEM) refers to a simulation technique where a fracture is modeled via splitting of special enriched finite elements during the course of a simulation. XFEM, unlike Cohesive Zone Method (CZM), allows simulating nucleation and growth of a fracture along an arbitrary, solution-dependent path without re-meshing the material in the bulk. In this work, we have used 2D XFEM coupled with pore-pressure degrees of freedom to simulate a variety of boundary value problems related to fluid-driven (hydraulic) fractures in a permeable medium. Specifically, through these simulations, we investigate the influence of critical geomechanical and operational parameters on hydraulic fracturing, including (a) creation of fracture-tortuosity due to a misalignment between initial perforation and maximum in-situ stress direction, (b) impact of in-situ stress anisotropy on the near-wellbore fracture geometry, (c) deflection of fracture path due to a spatial pore-pressure gradient, (d) refracturing of an already existing hydraulic fracture, and (e) merging of a hydraulic fracture with a pre-existing natural fracture in the formation. For each of these cases, the predicted fracture geometry is compared with the respective experimental result available in the literature. The simulated and the measured fracture geometries are found to be in good agreement.*

## 1. introduction

Hydraulic fracturing refers to the process of nucleation and growth of fractures inside rock formations by means of flow-induced pressurization (Hubbert and Willis, 1957; Khristianovic and Zheltov, 1955). Hydraulic fracturing is primarily used in the oil and gas industry as a means of stimulating unconventional reservoirs. Examples of unconventional reservoirs include oil and gas shales, tight sandstones, and heavy oil and tar sands. The ease of recovery of hydrocarbons from a given reservoir depends upon the mobility of the hydrocarbons in that reservoir, which is defined as the ratio of formation permeability to the viscosity of the host fluid (hydrocarbons). The mobility of hydrocarbons in unconventional reservoirs is typically several orders of magnitude smaller than that in conventional reservoirs. Because of such ultra-low mobility, the recovery of hydrocarbons from such reservoirs is much more challenging compared to a conventional reservoir. Therefore, often an assertive recovery method such as hydraulic fracturing is required to make the extraction of hydrocarbons from such reservoirs economically viable. Hydraulic fracturing facilitates the recovery of hydrocarbons from unconventional reservoirs by creating conductive channels which provide an easier escape route for the hydrocarbons.

Knowledge of the fracture trajectories resulting from a stimulation treatment can assist in determining the effectiveness of the treatment. For example, if an early diagnostic reveals undesired fracture growth or fault activation, the operators may utilize such information to terminate the treatment or to take a preventive measure. Field measurement techniques, such as micro-seismic monitoring, acoustic measurements etc., allow measuring hydraulic fracture paths directly in a field. However, such measurements are extremely expensive, rendering them economically unviable for diagnostic usage on a routine basis. Furthermore, micro-seismic measurements lack the resolution to accurately measure the near borehole features of a hydraulic fracture e.g. tortuosity, multi-stranded fractures etc.

Fracture trajectories resulting from a hydraulic fracturing treatment can be very complex. Often, such complexity arises due to interplay between geomechanical and operational factors. For example, triaxial fracturing experiments (Chen et al., 2010) have shown that the orientation of perforation tunnels relative to the maximum principal stress ($S_{\mathrm{hmax}}$) direction has a major influence on the near borehole fracture trajectory. When the perforations are oriented along the $S_{\mathrm{hmax}}$ direction, the resulting fractures are planar in geometry, i.e., free from any tortuosity. However, when the perforations are not aligned with the $S_{\mathrm{hmax}}$ direction, the resulting fractures initially open along the perforations but then quickly turn to align with the $S_{\mathrm{hmax}}$ direction, creating a non-planar, tortuous path. Studies have shown that near borehole tortuosity can adversely affect the flow of both fracturing fluid and hydrocarbons through hydraulic fractures (Clearly et al., 1993; Romero et al., 2000). Thus, near borehole tortuosity may have serious implications for the effectiveness of a stimulation treatment.

Hydraulic fracture paths are also sensitive to any spatial non-uniformity in pore pressure field. Spatial variations in pore pressure field may either be naturally present in the subsurface or may have been caused as a result of an industrial operation. For example, matrix reinjection of produced water and cutting slurry in the subsurface is a common disposal practice in oil/gas industry. The injection of an external fluid into the matrix can significantly alter the pore-pressure field in the subsurface, creating local regions of elevated pore pressure. Another example is depletion of hydrocarbons from the subsurface during a production process. The depletion creates local regions of lower pore pressure. Experimental studies (Bruno and Nakagawa, 1991) have shown that a hydraulic fracture, upon encountering a region of non-uniform pore pressure, may deflect towards it if it happens to be a region of elevated pore pressure, and may deflect away from it if it happens to be a region of lower pore pressure.

Pre-existing discontinuities such as faults and natural fractures are common in the subsurface. During the course of a stimulation treatment, natural fractures can interfere with a propagating hydraulic fracture in a variety of ways. Studies have shown that interference between a propagating hydraulic fracture and pre-existing discontinuities can significantly affect the trajectory of the hydraulic fracture. For example, Warpinski and Teufel (Warpinski and Teufel, 1987) showed that the interference of a hydraulic fracture with pre-existing fractures can result in a multi-stranded, non-planar fracture network. Blanton ((Blanton, 1982), using triaxial fracturing experiments, investigated the various ways a hydraulic fracture can interact with a natural fracture. He showed that, upon encountering a natural fracture, a hydraulic fracture can get arrested, or can merge and divert, or can cut through the fault.

A numerical simulation method such as Finite Element Analysis (FEA) may offer a reliable and economical means of assessing and predicting the location, direction and extent of hydraulic fractures. There are two major fracture modeling techniques that exist within the framework of FEA: Cohesive Zone Method (CZM) and Extended Finite Element Method (XFEM). CZM is based on the cohesive zone concept of Dugdale and Barenblatt (Barenblatt, 1959; Barenblatt, 1962; Dugdale, 1960). CZM assumes that the fracture takes place over a region of finite length instead of a singular crack-tip. In CZM, the fracture is modeled via special zero thickness elements in conjunction with a traction-separation relation (Chen et al., 2009; Carrier and Granet, 2012; Bao et al., 2016). However, CZM suffers from a major limitation: the fracture path in CZM needs to be assigned in advance, severely limiting the predictive capability of this technique. As a result, the applicability of CZM is limited only to cases where the fracture path is trivial and can be guessed in advance.

XFEM (Belytschko and Black, 1999; Moes et al., 1999; Lecampion, 2009) is a relatively new technique where a fracture is modeled via splitting of special enriched finite elements during the course of a simulation. XFEM allows a fracture to grow along an arbitrary, solution-dependent path without re-meshing the material in the bulk. For this reason, XFEM can be an ideal technique for modeling complex fracturing phenomena such as hydraulic fracturing, where the fracture trajectory is not known in advance. However, to the authors' knowledge, there has not been any systematic study demonstrating the applicability and validity of XFEM simulations in modeling of hydraulic fractures. The current work undertakes this task. The goal is to demonstrate the applicability and validity of XFEM simulations in modeling of fluid-driven fracture under a variety of different geomechanical and operational conditions. Towards this end, we simulate several operationally relevant cases of fluid-driven fractures and compare the simulated fracture geometries with the corresponding experimental results available in the literature. The considered boundary value problems examine how various geomechanical and operational parameters affect the fracture trajectories resulting from a hydraulic fracturing treatment. It will be demonstrated that XFEM simulations can reliably predict all the major features of fracture geometries in each of the considered scenarios.

The outline of this paper is as follows. In Sec. (2), we summarize the governing equations and constitutive relations describing the various processes associated with fluid-driven fractures. Sec. (3) discusses the various boundary-values problems related to fluid-driven fractures considered in this work: in Sec.(3.1), we simulate creation of a tortuous hydraulic fracture due to a misalignment between the perforation tunnel and the local $S_{\mathrm{hmax}}$ direction ; in Sec. (3.2), we investigate the issue of fracture path deflection due to a pore pressure gradient; in Sec. (3.3) we examine the impact of *in situ* stress contrast on near borehole geometry of hydraulic fracture; in Sec. (3.4) we simulate the refracturing of an already existing fracture, and in Sec.(3.4), we examine the interaction of an advancing hydraulic fracture with a pre-existing fracture in the formation. The article is concluded in Sec. (4) with a summary of the observations and findings noted in this work.

## 2. Governing equation

Mechanistically speaking, hydraulic fracturing involves coupling between the following four physical processes: (1) flow of the fracturing fluid within the fracture, (2) flow of the pore fluid within the formation, and leak-off of the fracturing fluid from the fracture into the formation, (3) deformation of the porous medium induced by both the hydraulic pressurization of the fracture and transport of the host fluid within the pores, and (4) fracture propagation which is inherently an irreversible and singular process. The governing equations and constitutive relations describing each of these physical processes are summarized in the following.

### 2.1 Elastic Deformation of the Matrix

The matrix is modeled as an isotropic, poroelastic material undergoing a quasi-static deformation. The equation of equilibrium in terms of total stress tensor is expressed as:

$$\nabla . \boldsymbol{\sigma} = 0 . \qquad (1)$$

The total stress tensor $\boldsymbol{\sigma}$ relates to the effective stress tensor $\boldsymbol{\sigma}'$ via the following relation (Terzaghi, 1925; Biot, 1941; Biot, 1955):

$$\boldsymbol{\sigma} = \boldsymbol{\sigma}' + \alpha P_p \boldsymbol{I} , \qquad (2)$$

where $\alpha$ is Biot's coefficient, $P_p$ is the pore pressure, and $\boldsymbol{I}$ is the identity tensor.

The constitutive equation, relating the effective stress tensor $\boldsymbol{\sigma}'$ to the strain tensor $\boldsymbol{\varepsilon}$, is given by:

$$\boldsymbol{\sigma}' = \lambda tr\boldsymbol{\varepsilon} + 2G\boldsymbol{\varepsilon} - \alpha P_p \boldsymbol{I} \;, \qquad (3)$$

where $\lambda$ and G are Lame` constants.

*2.2 Pore Fluid Flow*

The continuity equation for the pore fluid is expressed as:

$$\frac{1}{M}\frac{\partial P_p}{\partial t} + \alpha \frac{\partial (tr\boldsymbol{\varepsilon})}{\partial t} + \nabla . \boldsymbol{v} = 0, \qquad (4)$$

where $\boldsymbol{v}$ is the seepage velocity of the pore fluid, and $M$ and $\alpha$ are Biot's modulus and Biot's coefficient, respectively.

The seepage velocity $\boldsymbol{v}$ relates to the pressure-gradient $\nabla P_p$ via Darcy's law, which is given by:

$$\boldsymbol{v} = -\frac{k_a}{\mu} \nabla P_p , \qquad (5)$$

where $k_a$ is the absolute permeability of the formation and $\mu$ is the dynamic viscosity of the host fluid.

Upon combining Eq. (4) and Eq. (5), the continuity equation becomes (Biot, 1941; Biot, 1955):

$$\frac{1}{M}\frac{\partial P_p}{\partial t} + \alpha \frac{\partial (tr\boldsymbol{\varepsilon})}{\partial t} = \frac{k_a}{\mu} \nabla^2 P_p . \qquad (6)$$

## 2.2 Fracturing Fluid Flow

The flow of the fracturing fluid within the fracture is described by lubrication theory (Batchelor, 1967). Lubrication theory describes the pressure-driven flow of a fluid along a narrow channel, also called Poiseuille flow, the governing equation for which is given by:

$$\boldsymbol{q} = -\frac{w^3}{12\mu_f} \nabla P_f , \qquad (7)$$

where $w$ is the fracture gap, $P_f$ is the pressure inside the fracture, $\boldsymbol{q}$ is fracturing fluid flux (per unit width).

Eq. (7) should be solved in conjunction with the equation of mass conservation, which is given by:

$$\frac{\partial w}{\partial t}+\nabla.\boldsymbol{q}+v_t+v_b=Q(t)\delta(x-x_0;y-y_0), \quad (8)$$

where $v_t$ and $v_b$ are the normal flow velocities through the top and the bottom surfaces of the fracture; $\mu_f$ is the dynamic viscosity of the fracturing fluid; $Q$ is the injection rate, and $\delta$ is the 2D Dirac delta function.

Seepage of the fracturing fluid into the formation is governed by a leak-off model, which is given by

$$v_t=C_t(P_f-P_p^t), \quad (9)$$

and

$$v_b=C_b(P_f-P_p^b), \quad (10)$$

where $P_p^t$ and $P_p^b$ are the pore pressures in the adjacent material on the top and the bottom surfaces of the fracture, respectively, and $C_t$ and $C_b$ are the respective leak-off coefficients.

### 2.3 Fracture Initiation and Propagation

In this work, we use XFEM in conjunction with 2D plane strain elements with pore pressure degrees of freedom (CPE4P) to model hydraulic fractures. The XFEM implementation in ABAQUS™ is based on the phantom node formulation (Song et al., 2006; Hansbo and Hansbo, 1994) whereby each enriched element contains phantom nodes superposed on the real nodes. Prior to fracture, each phantom node is completely constrained to its corresponding real node. Once the fracture criterion is reached within an element, a copy of the element, which comprises of some real nodes and some phantom nodes, is generated (see Figure 1). The location of the fracture is tracked by means of a level set function $f(x)$.

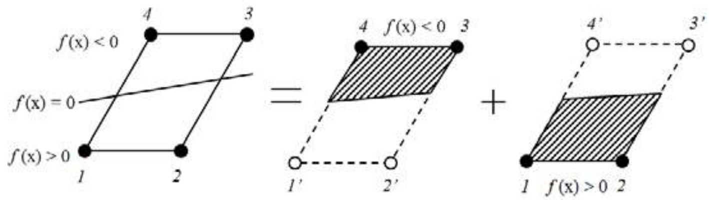


**Figure 1: Conceptual illustration of the principle of phantom node method. The solid circles denote the real nodes and the hollow circles are phantom nodes.**

The magnitude of separation is governed by a cohesive law until the cohesive strength of the cracked element is zero, after which the phantom and real nodes move independently. For the purpose of this study, we have employed a linear cohesive law, a schematic of which is shown in Figure 2.

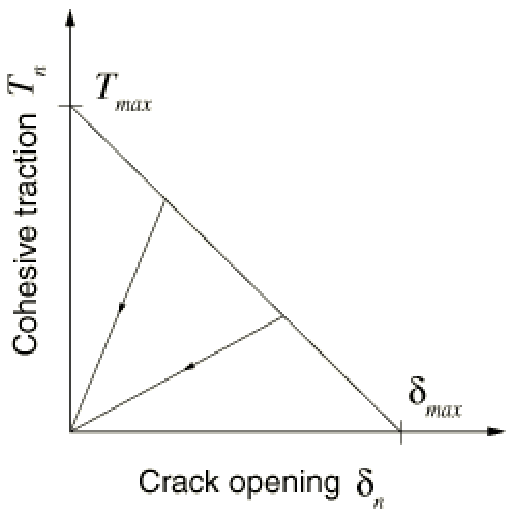


**Figure 2: Traction-separation response for cohesive behavior of an XFEM enriched element.**

## 3. Results and Discussion

### 3.1 Near Borehole Fracture Tortuosity

During a hydraulic fracturing stimulation treatment, the fractures nucleate from perforation tunnels that are shot along and around the borehole. The perforation tunnels, in general, are not aligned with the local *in-situ* maximum stress direction. Therefore, a hydraulic fracture nucleated from such a perforation tunnel may have to undergo reorientation until it is aligned with the *in-situ* maximum stress direction. Such reorientation results in a non-planar fracture growth in the near borehole region. The non-planarity in the fracture growth is called tortuosity. Fracture tortuosity can adversely affect the effectiveness of a hydraulic fracturing treatment. For example, in the presence of tortuosity, the overall treatment pressures are higher. Furthermore, in highly tortuous hydraulic fractures, the fracture conductivity is substantially reduced, constricting the flow of the fracturing fluid as well as hydrocarbons through such fractures. The tortuosity of a hydraulic fracture, in addition to mismatch angle, also depends on operational parameters such as injection rate and viscosity of the fracturing fluid (Zhang et al., 2011). Therefore, a predictive assessment of probable tortuosity during a hydraulic fracturing treatment can prove useful in selecting an optimal set of operational parameters for the given treatment.

Chen et al. (Chen et al., 2010) studied the propagation behavior and geometry of hydraulic fractures originating from oriented perforations in a triaxial fracturing test. The testing set-up comprised a cubical block of side 30 cm in length with a borehole of diameter 20 mm and a perforation tunnel 30 mm in length. The perforation tunnel was chosen to be oriented at an angle of $60^{o}$ with respect to the *in-situ* $S_{hmax}$ direction.

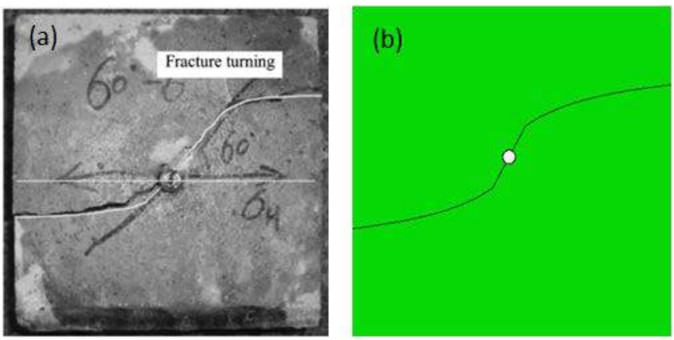


**Figure 3: (a) Experimental fracture trajectory from Chen et al. (Chen et al., 2010). (b) Fracture trajectory obtained from XFEM simulations.**

XFEM simulations show that the hydraulic fracture, post nucleation, reorients and quickly aligns with the $S_{hmax}$ direction, creating an S-shaped fracture trajectory. The simulated fracture trajectory, shown in Figure 3(b), appears to be in good agreement with the one observed in Chen et al.'s triaxial fracturing experiments, shown in Figure 3(a).

### 3.2 Effect of Stress Contrast on Near Borehole Fracture Trajectory

The governing principle for growth of hydraulic fractures is minimization of hydraulic energy, which requires that a hydraulic fracture should open against the minimum horizontal principle stress $S_{\text{hmin}}$. This makes $S_{\text{hmax}}$ direction the preferred direction for growth of hydraulic fractures. The difference between the two principal stresses is called the stress contrast. The stress contrast in a given area may be large or small depending upon the tectonic stresses in that area. The stress contrast can have significant implication for the near borehole geometry. For example, a vanishing stress contrast means a lack of preferred direction for fracture growth while high stress anisotropy means a distinct preferred direction for fracture propagation. In the discussion that follows, we examine how the stress contrast affects the near borehole fracture geometry resulting from a hydraulic fracturing treatment.

First, we consider an isotropic stress configuration, i.e. when the difference between $S_{\text{hmax}}$ and $S_{\text{hmin}}$ is zero. Experiments and XFEM simulations both show that in the absence of a stress contrast, there is no unique preferred direction for fracture growth and, as a result, upon injection, several fractures simultaneously nucleate at the borehole, as shown in Figure 4. Our simulations also show that not all the fractures continue to grow as the injection is continued; most of the fractures are prevented from growing due to stress shadowing from the surrounding fractures, and only a few continue to grow.

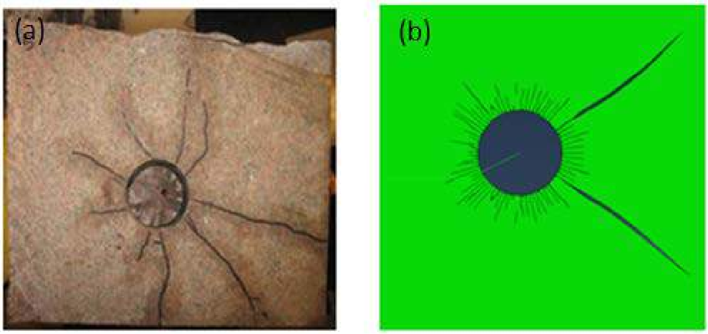


**Figure 4: Fracture geometry in an isotropic stress configuration ( $S_{\text{hmax}} = S_{\text{hmin}}$ ): (a) Experimental result from Frash (Frash, 2007) and (b) XFEM simulated fracture geometry from this work. There is no preferred direction for fracture propagation. As a result, a multitude of fractures simultaneously initiate at the borehole.**

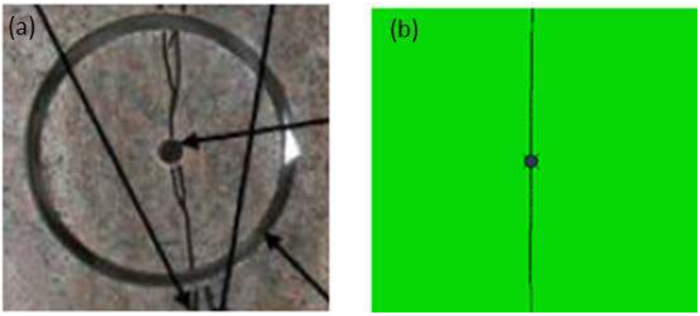


**Figure 5: Fracture geometry for an anisotropic stress configuration, i.e., when $S_{\text{hmax}} > S_{\text{hmin}}$: (a) Experimentally observed fracture trajectory from Frash (Frash, 2007), and (b) XFEM-simulated fracture trajectory. In this scenario, there is a distinct fracture growth direction (given by the direction of maximum principle stress), and accordingly a distinct, single fracture is observed in this case.**

On the other hand, in a distinctly anisotropic stress configuration, i.e., when the stress contrast is high, a distinct, single fracture aligned along the local $S_{\text{hmax}}$ direction is obtained. Experimental result on this is shown in Figure 5(a) and the XFEM simulation result is shown in Figure 5(b), both of which are in reasonable agreement.

### 3.3 Fracture Deflection due to Spatial Gradients in Pore Pressure

Often hydraulic fracturing treatments are carried out in regions where the prevailing pore pressure field is spatially non-uniform. Such spatial non-uniformity in pore pressure may have been caused either by the depletion of the host fluid from the reservoir (such as during production of hydrocarbons) or by the matrix injection of an external fluid into the subsurface (such as during produced water re-injection or cutting re-injection).

Bruno and Nakagawa (Bruno and Nakagawa, 1991) studied the influence of a spatially varying pore pressure field on hydraulic fracture propagation by means of triaxial fracturing experiments. Their experiments comprised a square slab of rock with multiple injection ports. The slab was subjected to a loading condition in which the maximum and minimum principal stresses were oriented along the north-south and east-west directions, respectively. First, a region of elevated pore pressure was created by injecting an external fluid into the matrix through one of the injection ports. Then, by injecting a fluid in a nearby port, a hydraulic fracture is nucleated and propagated. They showed that a spatial gradient in pore pressure can act as a body force, causing the hydraulic fracture to deflect towards the injected region, as shown in Figure 6(a).

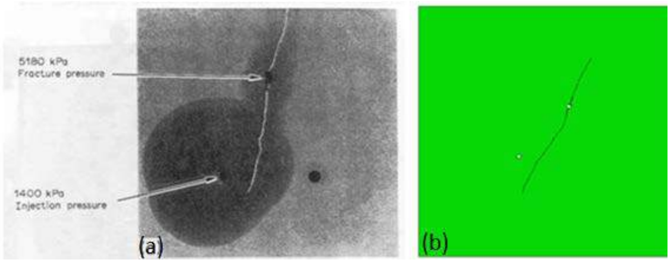


**Figure 6: Fracture deflection due to spatial gradient in pore pressure (a) as seen in Bruno and Nakagawa's experiments, and (b) as seen in XFEM simulations.**

Shown in Figure 6(b) is the fracture trajectory obtained from XFEM simulation of Bruno and Nakagawa's experiment. The simulated fracture trajectory shows that the hydraulic fracture is indeed attracted towards the region of elevated pore pressure, in conformation with  Bruno and Nakagawa's observations.

The contours of pore pressure and maximum principal stress in the post-injection state are shown in Figures 7(a) and 7(b), respectively.  Evidently, the matrix injection causes a significant alteration in the *in situ* stress field. In the discussion that follows, we delineate the mechanistic reasoning behind this injection-induced alteration of the *in situ* stress field

The upper bound on the compressive hoop stress around a borehole is given as (Malvern, 1969; Zoback, 2007):

$$S_{\theta\theta} = 3S_{\mathrm{hmax}} - S_{\mathrm{hmin}} + T - P_p - P_{BH} \ , \tag{11}$$

where $S_{\mathrm{hmax}}$ and $S_{\mathrm{hmin}}$ are the maximum and minimum compressive stresses (total), respectively; $P_p$ is the formation *in-situ* pore-pressure, and $P_{BH}$ denotes the borehole pressure.

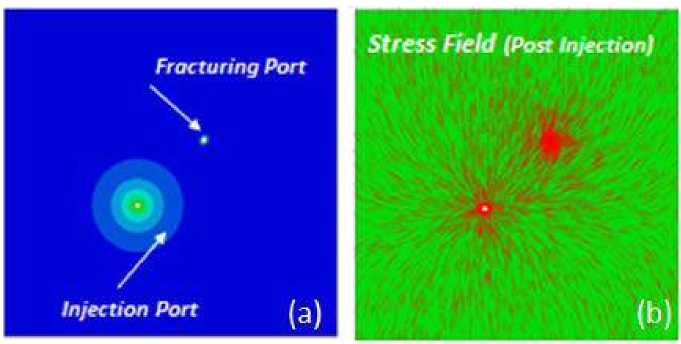

**Figure 7: (a) The contours of pore pressure showing local elevation in pore pressure due to matrix injection. (b) The contours of the altered maximum compressive principal stress. Originally, the maximum principal stress was oriented along the north-south direction.**

The compressive radial stress around the borehole is given by:

$$S_{rr} = P_{BH} - P_p . \tag{12}$$

Upon examining Eq. (11) and Eq. (12), we identify the following mechanism as responsible for the alteration of stress field. During matrix injection, the borehole pressure is set at a value higher than the formation *in-situ* pore pressure, i.e., $\Delta P = P_{BH} - P_p > 0$. The net pressure difference pushes the formation radially outward, subjecting the material around the borehole to an incremental tensile stress in the hoop direction and an incremental compressive stress in the radial direction. Thus, the net effect of subjecting the borehole to a positive net pressure is a reduction in the compressive hoop stress and an increase in the radial compressive stress. As the injection pressure is ramped up, the hoop stress becomes less and less compressive and the radial stress becomes more and more compressive. Once the injection pressure becomes sufficiently high, we can expect the hoop stress $S_{\theta\theta}$ to become the minimum compressive principal stress (or equivalently, the radial stress $S_{rr}$ to become the maximum compressive principal stress) in the region around the borehole.

We close the discussion on spatially non-uniform pore pressure field by simulating a scenario corresponding to depletion of hydrocarbons from a reservoir. The process of depletion is simulated by applying a suction at the borehole, i.e. by setting the borehole pressure to a value lower than the formation pore pressure, i.e., $\Delta P = P_{BH} - P_p < 0$. The fracture trajectory obtained from XFEM simulations for this case is shown in Figure 8(b). Evidently, the hydraulic fracture in this scenario moves circumferentially away from the region of reduced pressure.

The contours of maximum principal stress before and after the depletion are shown in Figure 8(c) and 8 (d), respectively. The depletion-induced alteration in the stress field can be explained as follows. The suction (negative net pressure) applied during the depletion pulls the formation radially inward, subjecting the material around the borehole to an incremental compressive stress in the hoop direction and an incremental tensile stress in the radial direction. Thus, with increasing suction, the radial stress becomes less and less compressive while the hoop stress becomes more and more compressive. Once the suction pressure becomes sufficiently high, the hoop stress $S_{\theta\theta}$ may become the maximum compressive principal stress (or equivalently, the radial stress $S_{rr}$ becomes the minimum compressive principal stress).

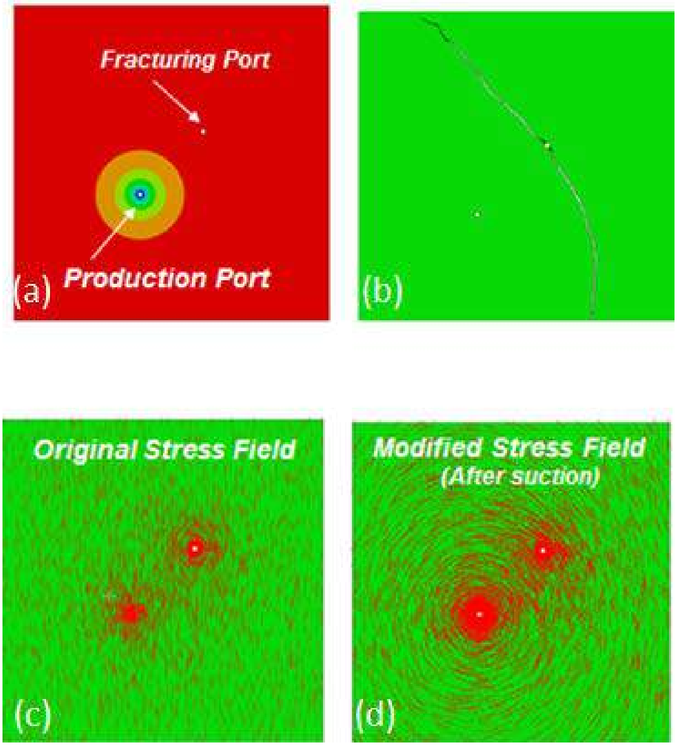


**Figure 8: (a) Contours of pore pressure in the post-depletion state. (b) XFEM simulated fracture geometry. (c) The contours of $S_{hmax}$ in the original state. (d) Modification of the stress field caused by depletion.**

### 3.4 Modeling of Refracturing Problem

Refracturing refers to an auxiliary stimulation technique where an already existing hydraulic fracture is plugged and re-injected with a fracturing fluid with the purpose of nucleating additional fractures. Since unconventional formations have an ultra-low permeability, the production rates in such formation declines much more rapidly compared to a conventional formation. The depletion is often limited to the near vicinity of fractures because of ultra-low permeability of these formations. In such reservoirs, a refracturing treatment may extend the production life of the reservoirs.

Shown in Figures 9(a) and 9(b) are the refracture geometries as obtained from the laboratory test of Liu et al. (Liu et al., 2008) and as predicted by XFEM simulations, respectively. XFEM simulations show that refracturing results in nucleation of a set of auxiliary fractures initially oriented in directions which differ from the in-situ $S_{hmax}$

direction. However, during the course of propagation, these refractures gradually reorient to align themselves with the *in-situ* $S_{\text{hmax}}$ direction.

The refracture trajectory obtained from XFEM appears to be in good agreement with the observed refracture geometry in Liu *et al.*'s experiments. However, the following exception needs to be noted. XFEM simulations predict four refractures in contrast to a single refracture observed in Liu *et al.*'s experiments. This is due to the fact that rocks, in reality, contain structural defects such as micro-cracks, micro-cavities and weak planes etc. which can act as preferred site for nucleation of fractures. However, in XFEM simulations, we do not assume any such structural defects and, as a result, there is no preferred site or direction for fracture nucleation in the simulations.

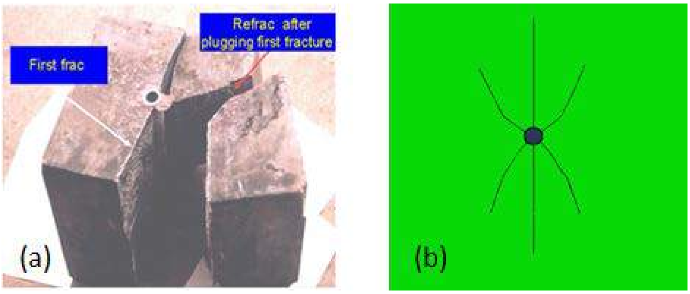


**Figure 9: (a) Experimental refracturing geometry (Liu *et al.,* 2008). (b) XFEM simulated refracturing geometry.**

### 3.5 Interaction of a Hydraulic Fracture (HF) with a Natural Fracture (NF)

Typically, unconventional reservoirs are naturally fractured, i.e. the underlying formations contain a myriad of pre-existing discontinuities in the form of fractures (also called natural fractures) and faults. These natural fractures act as fluid conduits, facilitating an easy flow of the hydrocarbons through the formation and hence improving the recovery of hydrocarbons. A natural fracture is also a weak plane in the formation which can be easily reactivated upon interaction with a hydraulic fracture. From a geomechanics point of view, the maximum compressive stress direction is the preferred growth direction for a hydraulic fracture. However, in the events of interaction between hydraulic fractures and natural fractures, the hydraulic fracture propagation may be governed by more than simply the confining stresses (Nagel and Sanchez-Nagel, 2015). Because a natural fracture provides an easy pathway for flow of the fracturing fluid, the interference between an advancing hydraulic fracture and a natural fracture may cause a significant diversion of the hydraulic fracture. Thus, in this way, interference with a natural fracture can also cause a more complex fracture trajectory and an increased treatment pressure.

Blanton (Blanton, 1982) investigated the interaction between a hydraulic fracture and a natural fracture using tri-axial fracturing experiments. Through these experiments, he examined the various ways a hydraulic fracture can interact with a natural fracture. He showed that, upon encountering a natural fracture, a hydraulic fracture can get arrested, or can merge and divert, or can cut through the natural fracture. In the following, we have simulated one such experiment examining the interaction between a propagating hydraulic fracture and a natural fracture using XFEM simulations. Our simulation, the result of which is shown in Figure 10 (b), indicates that, upon encounter, the hydraulic fracture merges with the natural fracture. This merger results in diversion of the hydraulic fracture away from its original propagation direction.

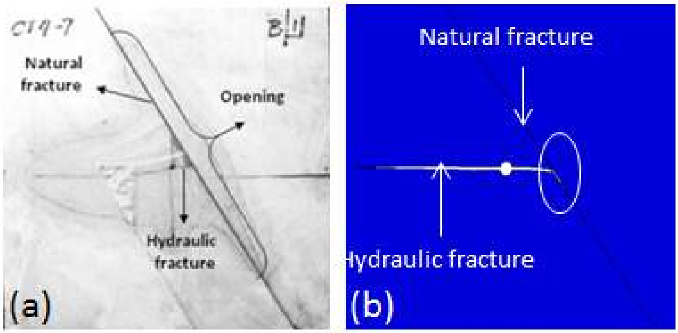


**Figure 10: (a) Fracture trajectory as obtained from Blanton's tri-axial experiments (Blanton, 1982). (b) XFEM simulated fracture trajectory, showing merging of the hydraulic fracture with the natural fracture. Subsequently, hydraulic fracture diverts away from its original propagation direction.**

## 4. conclusions

Several boundary value problems related to fluid-driven fractures have been discussed and simulated using XFEM. The simulations were validated by comparing their results with the respective experimental results available in the literature. The simulation results for individual boundary value problems are summarized as follows:

- XFEM simulations showed that in the event of a misalignment between perforation tunnels and maximum compressive stress direction, the fracture undergoes a re-orientation, and, as a result, the resulting trajectory tends to non-planar and tortuous.

- Our simulations correctly predicted the near borehole fracture geometry both for low and high stress contrast configurations. For the limiting case of vanishing stress contrast, the simulations showed a multi-stranded fracture whereas in high stress contrast configurations, a distinct, single fracture oriented along the *in-situ* $S_{\text{hmax}}$ direction was predicted.
- XFEM simulations showed that a spatial gradient in pore pressure can drastically modify the *in situ* stress field, and can cause a hydraulic fracture to deviate from its original path. For the specific case of matrix injection considered in this work, XFEM simulations showed that the hydraulic fracture is attracted towards the region of elevated pore pressure created by injection.
- For the refracturing problem, the simulations showed that refracturing results in nucleation of a set of auxiliary fractures initially oriented in directions which differ from the *in-situ* $S_{\text{hmax}}$ direction. However, during the course of propagation, these refractures gradually reorient to align themselves with the *in-situ* $S_{\text{hmax}}$ direction.
- For HF-NF interaction problem, the XFEM simulations predicted that the hydraulic fracture merges with the natural fracture, resulting in diversion of the hydraulic fracture away from its original propagation direction. This result is consistent with Blanton's observations based on triaxial fracturing experiments (Blanton, 1982).

For all the cases considered, the simulation results were found to be in good agreement with the respective experimental observations, establishing that XFEM simulations can reliably predict complex fracture trajectories under a variety of geomechanical and operation conditions. Through this work, we have demonstrated the applicability of XFEM in simulating a wide variety of boundary value problems related to fluid-driven fractures. The insights gained from these simulations will not only enhance our fundamental understanding of hydraulic fracturing but will also assist in the process of scientifically informed decision-making.

## 5. ACKNOWLEDGEMENT

The authors are grateful to Pablo Sanz and Fuping Zhou for many useful discussions.

## 6. References

1. Hubbert, M., and D. Willis. 1957 Mechanics of hydraulic fracturing. Petrol. Trans. AIME 210: 153-168.
2. Khristianovic, S. A., and Y. P. Zheltov. 1955. Formation of vertical fractures by means of highly viscous liquid. Proc. 4th World Petro. Cong. 579-586.

3. Zoback, M. D. 2007. *Reservoir Geomechanics* (First edition, Cambridge University Press, Cambridge (UK).
4. Malvern, L.E., 1969. *Introduction to the Mechanics of a Continuous Medium*, Prentice-Hall (UK).
5. Batchelor, G. K. 1967. *An Introduction to Fluid Dynamics.* Cambridge University Press, London.
6. Chen, M., H. Jiang, G. Q. Zhang, and Y. Jin. 2010. The Experimental Investigation of Fracture Propagation Behavior and Fracture Geometry in Hydraulic Fracturing through Oriented Perforations. *Petro. Sci. Tech.* 1297-1306.
7. Bruno, M. S., and F. M. Nakagawa. 1991 Pore pressure influence on tensile fracture propagation in sedimentary rock. *Int. J. Rock Mech.* 28: 261-273.
8. Terzaghi, C. 1925. Principles of Soil Mechanics, IV — Settlement and consolidation of clay. *Engineering News-Record* 95: 19-27.
9. Biot, M. A. 1941. General theory of three-dimensional consolidation. *J. Appl. Phys.* 12: 155-164.
10. Biot, M. A. 1956. General solutions of the equations of elasticity and consolidation for a porous material. *J. Appl. Mech.* 78: 91-96.
11. Biot, M. A. 1955. Theory of elasticity and consolidation for a porous anisotropic solid. *J. Appl. Phys.* 26: 182-185.
12. Cleary,M. P., D. E Johnson, and H. H. Kogsboll. 1993. Field implementation of proppant slugs to avoid premature screen-out of hydraulic fractures with adequate proppant concentration. SPE Paper No. 25892. In *SPE Rocky Mountain Regional/Low Permeability Reservoirs Symposium*, Denver, CO, 12–14 April.
13. Romero, J., M.G. Mack, and J.L. Elbel. 2000. Theoretical model and numerical investigation of near-wellbore effects in hydraulic fracturing. *Production and Facilities.* 15:76–82.
14. Dugdale, D.S. 1960. Yielding of steel sheets containing slits. *J. Mech. Phys. Solids.* 8: 100-104.
15. Barenblatt, G.I. 1959. The formation of equilibrium cracks during brittle fracture: general ideas and hypothesis, axially symmetric cracks. *J. Appl. Math. Mech.* 23: 622-636.
16. Barenblatt, G.I. 1962. The mathematical theory of equilibrium cracks in brittle fracture. *Advances in Applied Mechanics*. 7: 55-129.
17. ABAQUS User's Manual, Version 6.17. 2017. Dassault Systémes Simulia Corp., Providence, RI.
18. Zielonka, M.G., K.H. Searles, J. Ning, S.R. Buechler, Z. Du, L. Xia, and C. Wohlever. 2015. An extended finite element method for hydraulic fracturing of fully saturated porous media. In *11th World Congress on Computational Mechanics*, Barcelona, Spain, 20-25 July.
19. Moes, N., J. Dolbow, and T. Belytschko. 1999. A finite element method for crack growth without remeshing. *Int. J. Numer. Meth. Engng.* 46: 131-150.
20. Lecampion, B. 1999. An Extended Finite Element for Hydraulic fracture problems. *Int. J. Numer. Meth. Engng.* 25: 212-133.
21. Belytschko T, and T. Black. 1999. Elastic crack growth in finite elements with minimal remeshing. *Int. J. Numer. Meth. Engng.* 45: 601–620.

**22.** Hansbo A, and P. Hansbo. 2004. A finite element method for the simulation of strong and weak discontinuities in solid mechanics. *Comp. Meth. Appl. Mech. Engng.* 193:3523–3540.

**23.** Zhang, X., Jeffrey, R.G., Bunger, A.P., and Thiercelin, M. 2011. Initiation and growth of a hydraulic fracture from a circular wellbore. *Int. J. of Rock Mech. Min. Sci.* 48, 984-995.

**24.** Frash, L. P. 2007. PhD. Thesis, Colorado State University.

**25.** Liu, H., Z. Lan, G. Zhang, F. Hou, X. He, and X. Liu. 2008. Evaluation of refracture reorientation in both laboratory and field scales. SPE-112445-MS. In *SPE International Symposium and Exhibition on Formation Damage Control*. Lafayette, Louisiana, 13-15 Feb.

**26.** Warpinski, N. R., and L. W. Teufel. 1987. Influence of geologic discontinuities on hydraulic fracture propagation. *J. Pet. Technol.* 39, 209-220.

**27.** Nagel, N.B., and M. A. Sanchez-Nagel. 2015. On the importance and impact of key geomechanical parameters in unconventional play developments. Paper ARMA 15-514 presented in 49th US Rock Mechanics/Geomechanics Symposium, San Francisco, CA, USA 28 June – 1 July 2015.

**28.** Blanton, T. L. 1982. An experimental study of interaction between hydraulically induced and pre-existing fractures. SPE-10847-MS. In *SPE unconventional gas recovery symposium.* Pittsburgh, PA, 16-18 May.